Article:
Beltran-Rendon, C., Price, C.J. orcid.org/0000-0002-5355-0546, Glen, K. orcid.org/0000-0002-7489-8808 et al. (3 more authors) (2024) Modeling the selective growth advantage of genetically variant human pluripotent stem cells to identify opportunities for manufacturing process control. Cytotherapy, 26 (4). pp. 383-392. ISSN: 1465-3249

https://doi.org/10.1016/j.jcyt.2024.01.010

Cytotherapy 26 (2024) 383–392

Contents lists available at ScienceDirect

CYTOTHERAPY

journal homepage: www.isct-cytotherapy.org

FULL-LENGTH ARTICLE
Manufacturing

Modeling the selective growth advantage of genetically variant human pluripotent stem cells to identify opportunities for manufacturing process control

Catherine Beltran-Rendon[1,#], Christopher J. Price[2,3,4,#], Katie Glen[1], Adrian Stacey[1], Ivana Barbaric[2,3,4,*], Robert J. Thomas[1,**]

[1] Centre for Biological Engineering, Loughborough University, Loughborough, UK
[2] School of Biological Sciences, The University of Sheffield, Western Bank, Sheffield, UK
[3] The Neuroscience Institute, The University of Sheffield, Western Bank, Sheffield, UK
[4] INSIGNEO Institute, University of Sheffield, Sheffield, UK

ARTICLE INFO

Article History:
Received 24 May 2023
Accepted 27 January 2024

Key Words:
computational model
cultured acquired genetically variant hPSCs
human pluripotent stem cell (hPSC)
manufacturing process control
process parameters

ABSTRACT

Background aims: The appearance of genetically variant populations in human pluripotent stem cell (hPSC) cultures represents a concern for research and clinical applications. Genetic variations may alter hPSC differentiation potential or cause phenotype variation in differentiated cells. Further, variants may have properties such as proliferative rate, or response to the culture environment, that differ from wild-type cells. As such, understanding the behavior of these variants in culture, and any potential operational impact on manufacturing processes, will be necessary to control quality of putative hPSC-based products that include a proportion of variant threshold in their quality specification.
Methods: Here we show a computational model that mathematically describes the growth dynamics between commonly occurring genetically variant hPSCs and their counterpart wild-type cells in culture.
Results: We show that our model is capable of representing the growth behaviors of both wild-type and variant hPSCs in individual and co-culture systems.
Conclusions: This representation allows us to identify three critical process parameters that drive critical quality attributes when genetically variant cells are present within the system: total culture density, proportion of variant cells within the culture system and variant cell overgrowth. Lastly, we used our model to predict how the variability of these parameters affects the prevalence of both populations in culture.

Introduction

Over the last several years, the rapid advancement of human pluripotent stem cell (hPSC)-derived cell therapies into clinical trials has moved the field of regenerative medicine closer to a new era of therapeutics [1–3]. However, key challenges remain surrounding the safe and reproducible expansion of cell therapies into defined large-scale manufacturing production capable of meeting the therapeutic demand [4,5]. Significant among these is to understand how genetic variability can affect the manufacturing system.

Manufacturing of a hPSC-derived cell therapy requires the expansion and maintenance of a genetically stable population of cells [4]. However, it is well established that hPSCs may acquire recurrent genetic abnormalities that commonly present as either copy number variants or gains of whole or regions of chromosomes; 1, 12, 17, 20 and X, upon prolonged culture [1,4–8]. In the pluripotent state, these acquired variants provide the abnormal cell with a selective growth advantage, enabling them to overtake wild-type cells in culture [7,9,10]. Although the potential impact of these mutations within the differentiated state of specific regenerative applications is not yet known, it is worth noting that most of the commonly observed genetic abnormalities have been related to different tumorigenic phenomena [4,5]. One of the predominant features typically displayed by variant hPSCs, which is also a complementary hallmark of cancer, is possession of a faster growth rate

* Correspondence: Ivana Barbaric, School of Biological Sciences, The University of Sheffield, Western Bank, Sheffield, UK.
** Correspondence: Robert J. Thomas, Centre for Biological Engineering, Loughborough University, Loughborough, UK.
E-mail addresses: i.barbaric@sheffield.ac.uk (I. Barbaric), R.J.Thomas@lboro.ac.uk (R.J. Thomas).
# These authors contributed equally to this work.

https://doi.org/10.1016/j.jcyt.2024.01.010

than their wild-type cells. Therefore, the appearance of genetically variant cells in culture creates a variable that has the potential to influence manufacturing outcomes. Understanding the dynamics of how abnormal cells arise and establish within cultures is essential for designing strategies of process control during the expansion of hPSCs for manufacturing purposes.

Previous studies have explored strategies to overcome the presence of genetically variant cells within an expanding culture. One strategy has been to identify culture conditions that can reduce the appearance of genetic variations. Maintaining cells in a hypoxic environment has been shown to reduce oxidative stress and thus prevent DNA mutation accumulation, offering a set of manufacturing parameters that might be operationally more favorable [11]. Alternative studies have explored identifying the mechanisms through which variant cells exploit and overcome the culture environmental constraints that limit normal hPSCs expansion, in order to control their proliferation [4,10,12]. However, the mechanisms that underpin this aspect of variant hPSCs advantage currently remain insufficiently defined to design a control strategy. Moreover, we have recently investigated the behavior of karyotypically diploid wild-type and genetically variant hPSCs when cultured together [10]; this study provided an understanding of variant cell behavior and robust experimental data that could support mechanistic analysis of the growth interaction between wild-type and genetically variant cells.

Here, we have applied a modeling technique previously developed and demonstrated to represent cell behavior in a manner appropriate for cell processing optimization [13–15]. This is a tailored ordinary differential equation (ODE)-based modeling framework that represents key mechanisms underpinning bioprocesses in terms relevant to process control variables with the use of strategically collected experimental data [13]. In this study, we sought to develop a model that could exploit the available data and current mechanistic understanding to predict the proliferation of variant and wild-type cells when cultured separately and together based on their innate properties and differential modulation of these properties by culture state such as density or cell-type population constitution. Our results show that the model is capable of representing the growth behaviors of wild-type and variant hPSCs in both independent and co-culture systems, and it defined three critical process parameters that determine the overgrowth rate of variant cells. Furthermore, we demonstrate how the model can be used to determine conditions that either inhibit or enhance the overtaking of variant cells. These findings have practical implications for the rapid detection of undesirable genetic variants and the quality control of hPSC-based cell therapies.

Methods

hPSC growth rate

Growth rate analysis was performed on two wild-type sublines (H7.S14 and H7-H2B-RFP) and two variant sublines (H7v1,17,i20 and H7v1,12,17,20q-GFP), as previously described [10,12]. In summary, before experiments, the cell banks of wild-type early passage sublines of the hPSC line H7 (WA07) [16] used in this study; H7.S14 and H7-H2B-RFP were characterized as karyotypically normal based on at least 20 metaphases analyzed by G-banding and did not possess the commonly gained 20q11.21 copy number variant as determined by florescent in situ hybridization and/or quantitative polymerase chain reaction for copy number changes [7,17]. The karyotypes of the H7 genetically variant sublines H7v1,17,i20 [47,XX, +del(1)(p22p22), der(6)t(6;17)(q27;q1), t(12;20)(q13;q11.2), i(20)(q10)dup(20) (q11.21q11.21) and H7v1,12,17,20q-GFP [48,XX, +del(1)(p22p22), der(6)t(6;17)(q27;q1), +12, ish dup (20q11.21q11.21)] were confirmed by G-banding of 30 metaphase spreads and 20q copy number variant in H7v1,12,17,20q-GFP determined by quantitative polymerase chain reaction analysis and florescent in situ hybridization. Human PSCs were cultured on Vitronectin (cat. no. A14700; Thermo Fisher Scientific, Waltham, MA, USA) and maintained in E8 medium prepared in-house, consisting of Dulbecco's Modified Eagle's Medium/F12 (cat. no. D6421; Sigma-Aldrich, St. Louis, MO, USA) supplemented with 14 μg/L sodium selenium (cat. no. S5261; Sigma-Aldrich), 19.4 mg/L insulin (cat. no. A11382IJ; Thermo Fisher Scientific), 1383 mg/L NaHCO3 (cat. no. S5761; Sigma-Aldrich), 10.7 mg/L transferrin (cat. no. T0665; Sigma-Aldrich), 10 mL/L Glutamax (cat. no. 35050038; Thermo Fisher Scientific), 40 μg/L FGF2-G3 (cat. no. Qk053; Qkine, Cambridge, UK) and 2 μg/L TGF-β1 PLUS (cat. no. Qk010; Qkine) [18].

Each population was grown independently and in co-culture, with the co-culture consisting of the mixture of wild-type cells and one of the variant sublines. Cells in the independent cultures were seeded at two different densities; 4.5×10^4 cells/cm^2 (higher density) and 2.25×10^4 cells/cm^2 (lower density), whereas co-cultures were seeded at 4.5×10^4 cells/cm^2 containing an equal proportion of each population (2.25×10^4 cells/cm^2). Cells were fed daily and maintained at 37°C under a humidified atmosphere of 5% CO_2 in air [12].

Modeling and model validation for manufacturing

Cell culture dynamics and their modulation were mathematically represented using the ODE-based modeling framework previously described [13]. This approach uses tailored ODEs and a limited range of additional functions selected from a constrained library of building blocks. The values of the parameters were optimized by simultaneously fitting experimental datasets to minimize least squares deviation (i.e., a brute force screen of all combinations of parameter values). Following Stacey *et al.* [13], a software interface was used in which each block graphically corresponds to a building block from the library and thereby represents a cell dynamic that is mathematically simulated by within the system of ODEs. The configurations selected in this study are represented in graphical schemes within the relevant section.

Underlying hypotheses were iterated in light of deviations between simulation results and real-life data (i.e., experimental data). An acceptable model fit was considered to show a strong correlation between simulation and experimental data (R^2) and no gross systematic deviations in residuals across the model experimental space. The degree of representation also was evaluated through the adjusted R^2, which penalizes for adding extra parameters in the model that do not necessarily explain the variation of the experimental data (i.e., representing data noise rather than the cell behavior). The best-fitting model was tested against independent data to validate representation and predictive capability (as further discussed).

Hypotheses modeled and tested are described conceptually to follow, including the correspond systems ODEs:

Hypothesis 1. (see "Modeling the independent growth behavior of wild-type and genetic variant cells"): Quiescent cells are converted to proliferative cells, proliferative cells grow exponentially with rate reduced as a function of proliferative cell density:

$$\frac{dQ}{dt} = -r_r Q \tag{1}$$

$$\frac{dP}{dt} = r_r Q + r_g S(P, g_c, g_s) P \tag{2}$$

where Q and P are, respectively, the densities of quiescent and proliferative cells, t is time, r_r is the rate at which quiescent cells become proliferative, r_g is the maximum growth rate for the proliferative cells and the sigmoidal function S models the reduction in proliferation as density increases, with a threshold g_c and sensitivity g_s. We use:

$$S(x; c, s) = \frac{1}{1 + e^{(x-c)s}} \tag{3}$$

Hypothesis 2. (see "Modeling the growth of wild-type and variant hPSCs in co-culture system"): As hypothesis 1, but two populations of quiescent cells are converted to proliferative cells of two types (wild-type and variant) and the growth rate of each is reduced as a function of the total density of proliferative cells.

$$\frac{dQ_1}{dt} = -r_{r,1}Q_1 \tag{4}$$

$$\frac{dQ_2}{dt} = -r_{r,2}Q_2 \tag{5}$$

$$\frac{dP_1}{dt} = r_{r,1}Q_1 + r_{g,1}S(P_1 + P_2, g_{c,1}, g_{s,1})P_1 \tag{6}$$

$$\frac{dP_2}{dt} = r_{r,2}Q_2 + r_{g,2}S(P_1 + P_2, g_{c,2}, g_{s,2})P_2 \tag{7}$$

where Q_1, Q_2, P_1 and P_2, respectively, are the densities of quiescent wild-type, quiescent variant, proliferative wild-type and proliferative variant cells; r_r, n is the rate at which quiescent cells of wild-type (n = *1) and variant* (n = 2) are converted to proliferative cells and all other variables and parameters are as defined for hypothesis 1.

Hypothesis 3. (see "Restructuring the model to account for the behavioral differences observed"): As hypothesis 2, but the wild-type growth rate comprises a part that is attenuated by the total proliferative cell density, and a second part that is attenuated only by the variant cell density:

$$\frac{dQ_1}{dt} = -r_{r,1}Q_1 \tag{8}$$

$$\frac{dQ_2}{dt} = -r_{r,2}Q_2 \tag{9}$$

$$\frac{dP_1}{dt} = r_{r,1}Q_1 + r_{g,1}S(P_1 + P_2, g_{c,1}, g_{s,1})P_1 + r_{h,1}S(P_2, g_x, g_y)P_1 \tag{10}$$

$$\frac{dP_2}{dt} = r_{r,2}Q_2 + r_{g,2}S(P_1 + P_2, g_{c,2}, g_{s,2})P_2 \tag{11}$$

where $r_{g,1}$ and $r_{h,1}$, respectively, are the fraction of the wild-type growth rate that depends on the total density and the variant density; g_x and g_y are the threshold and sensitivity of the growth rate dependency on the variant density and all other variables and parameters are as defined for hypothesis 2.

The values describing the variability of the culture in "Manufacturing operational consequence of the model" were calculated from a time series of cell densities generated by simulating the conditions in Table 1 in the best-fitting co-culture model with the parameter values of Table 4. Then, these data were used to calculate the culture density, proportion of variants and the variant overgrowth rate ($\triangle\mu$) (Equation 12 and Equation 13). $\triangle\mu$ was calculated as the difference between the variant and wild-type growth rate, where μ represents the growth rate, N is the density, and t is the time.

$$\text{Variants}_i(\%) = \frac{N_{\text{Variants}_i} \cdot 100\%}{N_{\text{Variants}_i} + N_{\text{wild-type}_i}} \tag{12}$$

$$\Delta\mu_i(h^{-1}) = \frac{\ln \frac{N_{\text{Variant } t_i}}{N_{\text{Variant } t_{i-1}}} - \ln \frac{N_{\text{wild-type } t_i}}{N_{\text{wild-type } t_{i-1}}}}{t_i - t_{i-1}} \tag{13}$$

Table 1
Experimental computational conditions analyzing the variability of the culture.

Condition	Variant initial density ($\times 10^4$ cells/cm^2)	Wild-type initial density ($\times 10^4$ cells/cm^2)
1	3.0	3.0
2	3.0	1.5
3	2.25	2.25
4	1.5	3.0
5	1.5	1.5

Results

To define the growth dynamics of wild-type and variant hPSCs during expansion in mosaic cultures, we first sought to develop a mechanistic growth model representing the behavior of both cell populations when grown independently. Using the wild-type and two variant sublines (v1,17q,i20 and v1,12,17,20q-GFP), we simulated characteristic behaviors cells exhibit across a standard culture to quantify their growth properties. Subsequently, the model was adapted to represent the co-culture scenario in which both populations exist and expand within the same culture system. The new model structure allowed us to assess how the growth behavior of both cell populations is altered compared with independent culture and subsequently define an additional inhibitory mechanism, exerted by variant hPSCs, that modulates the growth dynamics of wild-type cells. Following validation of the best-fitting model structure by degree of representation to a new data set, we used our model to examine how specific culture parameters could alter the growth dynamics of both wild-type and variant cell populations and ultimately define the variant cells overgrowth rate.

Modeling the independent growth behavior of wild-type and genetic variant cells

Using the ODE modeling framework, characteristic behaviors exhibited across a standard culture were simulated to study the independent growth behavior of wild-type and variant cell populations. The model structure was based on hypothesized key cell dynamics: first, after seeding, cells change from a non-proliferative to a proliferative state. Afterwards, the cells begin dividing at regular intervals until, lastly, becoming inhibited by the cell density (daily medium exchange was applied to prevent medium limitations) (Figure 1A). The number of cells in a non-proliferative or proliferative state was represented as independent species, shown as oval-shaped modules, and their modeled dynamics were represented by equations indicated by square modules. Parameters associated with each equation are defined next to them in italic square modules (Figure 1B).

To optimize the model parameters for our wild-type and two variant sublines, we simultaneously fitted experimental data from each population, acquired across regular time points from cell seeding (24 h) over a 3-day culture period (96 h). In the simulation data, we observed that the model output appropriately represented the wild-type and variants growth behavior, with low sensitivity to capture data noise (Figure 1C–E). The simulation results displayed a strong correlation to the experimental data (R^2 = 0.96 and adj. R^2 = 0.96), and no systematic patterns were observed in the residual values (Figure 1F). Collectively, these observations indicate the same model structure can be used to represent the growth behavior of wild-type and variant sublines when cultured independently. Moreover, differences in the fitted parameter values between the populations indicate that the enhanced growth properties of variant hPSCs are likely due to a faster growth rate and not differences in their ability to initiate proliferation after seeding, for example (Table 2).

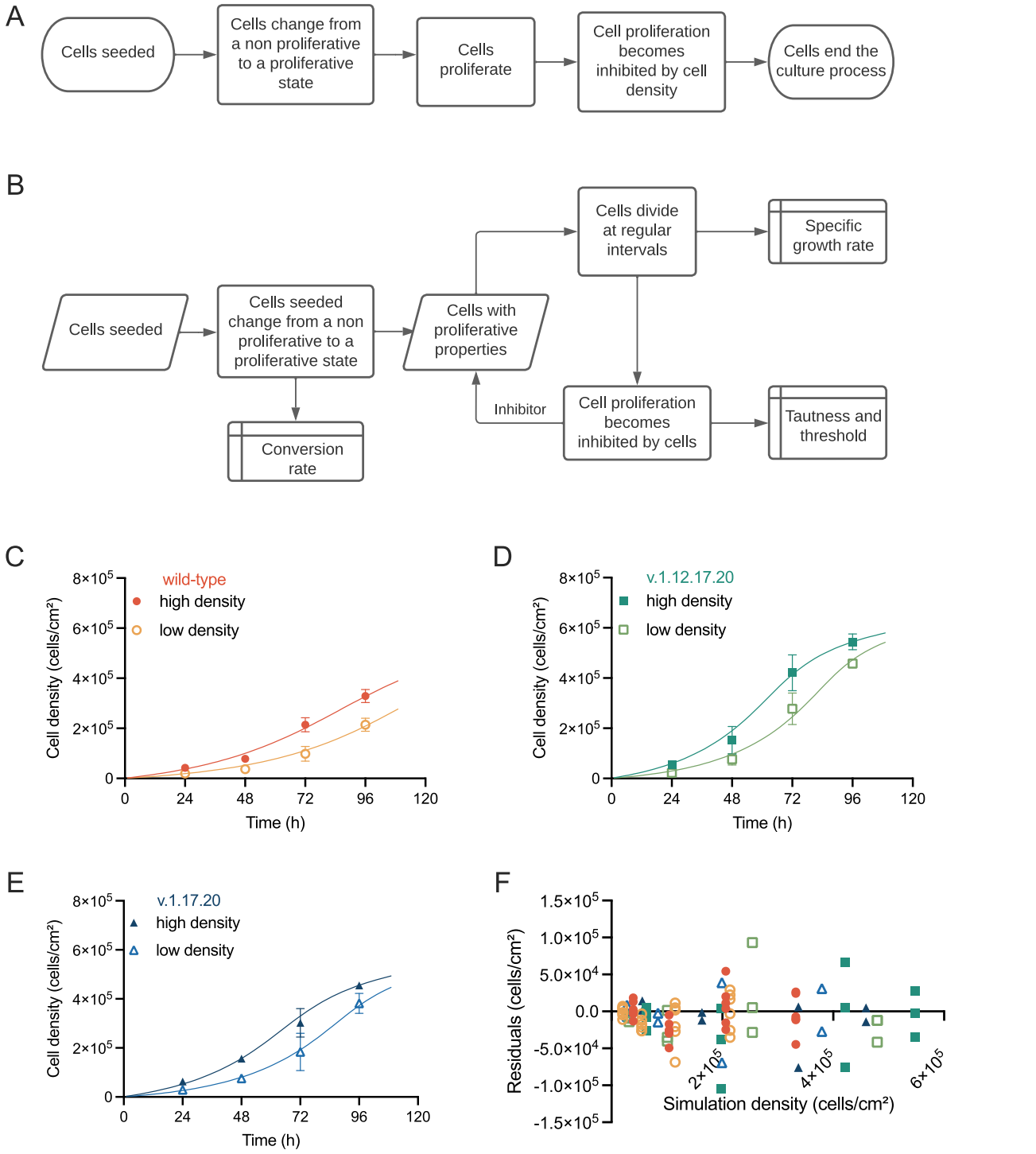

Figure 1. (A) Biological behavior aimed to be represented in the independent growth model, and (B) description of the software building blocks representing the behavior. Simulation results (line) and experimental cell count (markers) across time for the (C) wild-type, (D) v.1.12.17.20 and (E) v.1.17.20 populations illustrate the model's degree of representation. N ≤ 6 and error bars are showing standard deviation. (F) Simulation results across residual values are low and show a lack of predictability. (Color version of figure is available online.)

Table 2
Table of fitted parameter values that characterize each population.

Cell line	Variable	Wild-type	v.1.12.17.20	v.1.17.20
Conversion of cell state rate, h^{-1}	Eq. 1, r_r	2	2	2
Growth rate, h^{-1}	Eq. 2, r_g	0.026	0.035	0.032
Inhibition threshold, $\times 10^5$ cells/cm^2	Eq. 2, g_c	3.9	4.7	4.1
Inhibition sensitivity, $\times 10^{-5}$ cm^2/cells	Eq. 2, g_s	1.0	1.5	1.5

Modeling the growth of wild-type and variant hPSCs in co-culture system

Given that when variant hPSCs arise they exist within the same culture environment as wild-type cells, we next adapted the growth model to represent a scenario in which a wild-type and a variant cell population grow together. We first hypothesized that in a simple scenario, both populations would behave in a similar manner to their respective independent cultures, with the exception that each population would now be inhibited by the total cell density of the system rather than their own individual densities (Figure 2A). To this end, we applied the independent growth parameter values previously described in Table 2 to the re-structured model (Figure 2B).

In the new simulations, we observed a high initial correlation to the experimental growth data at early time points, which was then followed by both populations systematically deviating from the model (R^2 = 0.88 and adj. R^2 = 0.83, Figure 2C–D). As such, the residual values displayed a pattern of predictability over the time, with underpredicted values for the variant populations and overpredicted values for the wild-type cells at the later stages of culture (Figure 2E–F). Systematic residual deviation at the end of the culture indicated an inaccurate representation of the mechanisms driving growth inhibition and, based on these findings, we concluded that total system density is solely insufficient to predict co-culture behavior of the wild-type and variant hPSCs and growth inhibition is driven by an interaction between populations.

Restructuring the model to account for the behavioral differences observed

Given that variant sublines v1,17q,i20 and v1,12,17,20q-GFP have been reported to have the capacity to competitively inhibit the growth of wild-type cells [10], we next simulated the suppressive effect experienced by the wild-type cells by altering the model to include an additional separate inhibition module in the wild-type growth rate that was modulated by the variant cells (Figure 3A–B). In the new model structure, both wild-type and variant populations continue to be inhibited by the overall system density, but wild-type cells possess a separate inhibitory parameter associated with the variant population, allowing the variant to exert an independent and additional inhibitory effect on the wild-type population. We hypothesized that in our new co-culture model, both cell types would retain some of their independent growth parameters (displayed in italics in Table 3) and the simulations were set to only optimize parameters that represented the wild-type cells growth rate, and their inhibition (displayed in bold in Table 3).

Simulated data showed that the restructured model was an improvement for appropriately representing the co-culture growth of both wild-type and variant cells, given the strong correlation to the experimental result (R^2 = 0.92 and adj. R^2 = 0.87) (Figure 3C–D). In addition, we observed that no residual values showed systematic patterns or predictability (Figure 3E–F). However, we noted residual values tended to increase within the variant populations at high densities, suggesting that in co-culture variants might also increase their growth rate with respect to the model prediction when cultured independent (Figure 3E–F).

Moreover, we found that the wild-type cell growth rate decreased compared with the previously calculated independent growth rate value (e.g., cond. 1 0.021 h^{-1} vs 0.026 h^{-1}, as seen in Table 3 and Table 2), indicating growth suppression due to the presence of the variants. As the specific growth rates represent the fraction of the growth inhibited by each of their modulators. In the wild-type cells, the specific growth inhibited by the presence of the variants is overall lower but occurs more quickly than the specific growth inhibited by cell density (i.e., confluence). Overall, these findings suggest that variant cells provide a suppressive effect that acts throughout the co-culture, although it is less impactful than the inhibition of wild-type growth that is caused by confluence, which occurs at the end of the culture period.

Model validation

Validation by representing a new data set

To validate our restructured model, we performed two assessments of model performance using wild-type hPSCs and variant subline v.1,12,17,20. First, we simulated the growth of both cell types across a range of seeding densities using the previously determined parameter values (Table 3) to evaluate whether the model could represent a new data set that was not used during its construction. A six-point seeding density series, with both populations contributing proportionally to the overall density (50:50), was used to simulate cell growth. Model performance was evaluated by comparing simulation results against experimental data acquired at 24-h and 96-h time points. These time points were selected based on the model characteristics to show early systematic deviation in growth rates relative to model prediction or changes in late-stage inhibition. In our simulation data, we observed the culture system acquired a higher proportion of variant cells and a lower proportion of wild-type as the overall density was increased, fitting with our previous observations (Figure 4A–B). Furthermore, the simulated data showed a strong correlation coefficient of R^2 = 0.94 for all density conditions (Figure 4C), and adj. R^2 = 0.93. However, although the simulation appropriately represented the behavior, simulations of the wild-type population started to underperform at low densities (Figure 4D–F), with values under-predicting its behavior at densities below 2×10^4 cells/cm^2 (also Figure 4A–B).

Optimizing the parameter values on a broader data set

Given the systematic deviation in the model residuals at low density, we combined all the previously used growth data to further optimize our parameter values against culture scenario's containing different ratios of variant hPSCs; 0%, 50% and 100%. We had previously shown that conversion of the cell state rate does not drive behavioral performance (Table 2 and Table 3); therefore, we excluded the parameter to reduce the model's complexity. Of note, we observed that the parameters optimized from the broader data set qualitatively replicated our previous growth rate observations despite showing small differences in their values (Table 4). The variant growth rate remained higher than the wild-type, and the specific wild-type growth rate inhibited by the variant population was lower and still occurred faster than the specific growth inhibited by the confluence state. Based on these results, we concluded that the model structure appropriately represents the co-culture behavior.

Lastly, we simulated the previously used six-point density series with the optimized parameters. Comparison with the experimental data showed that the model results appropriately represented the behavior (R^2 = 0.94, Figure 4G–H, and adj. R^2 = 0.93), although underpredicted values were still visible at low densities (Figure 4I–K). Moreover, we did notice an improved representation of the wild-type population across low densities with the new parameter values relative (Figure 4L) to the previous (Figure 4C).

Manufacturing operational consequence of the model

Our model representation revealed that as a consequence of variant hPSCs possessing a faster growth rate than their wild-type counterparts, as overall culture density increases, there is also a greater increase in the proportion of variant cells over wild-type cells in the system. Thus, variability within the culture can be defined by the following variables: variant overgrowth rate, overall density and proportion of variants in culture. To gain further insight into the interaction of these three variables and to identify strategies for

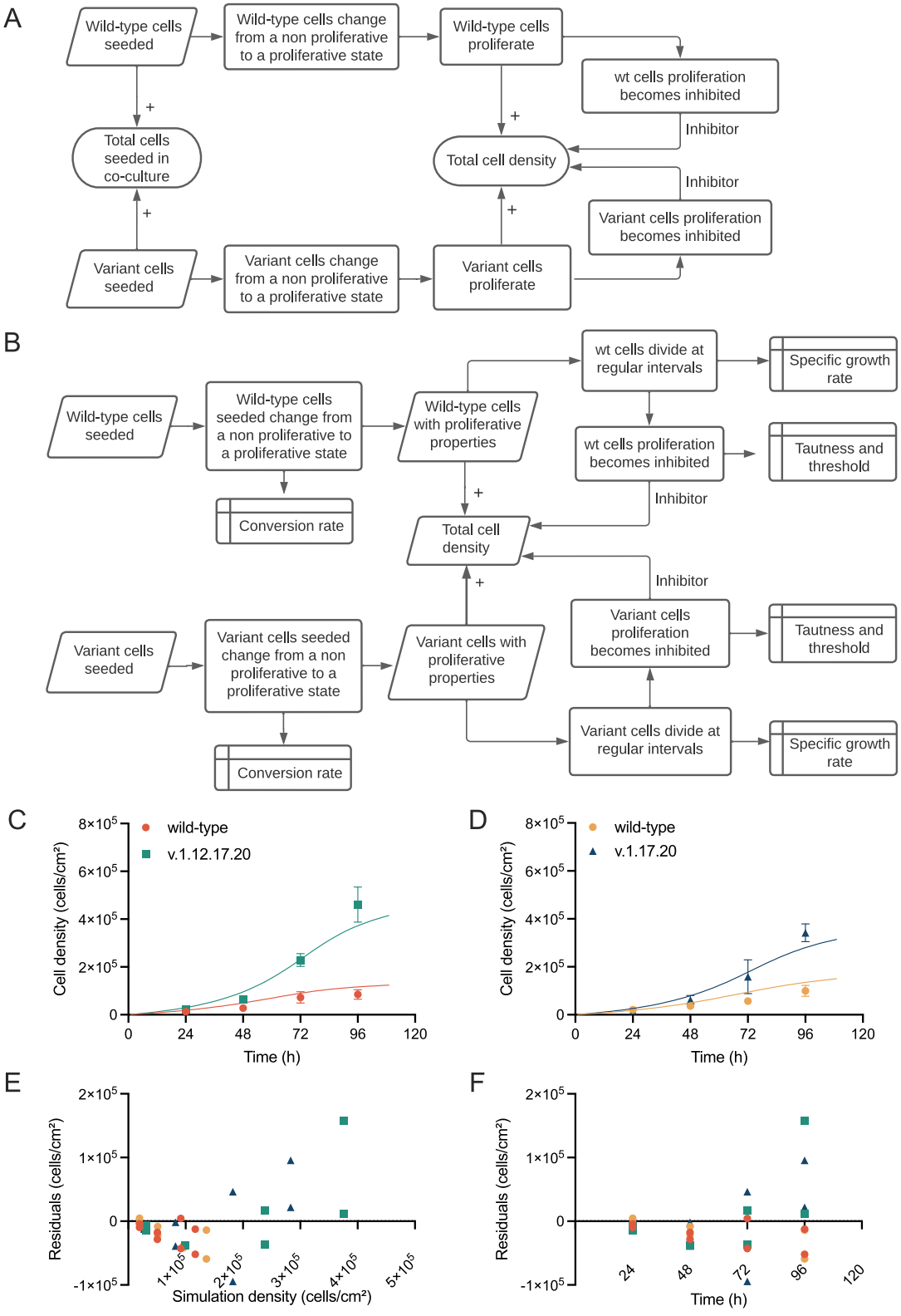

Figure 2. (A) Biological behavior represented with overall density as growth inhibitor and (B) software building blocks representing the behavior. Simulation results (line) and experimental counts (markers) versus time for the co-culture of the (C) wild-type and v.1.12.17.20 and (D) wild-type-RFP and v.1.17.20. N = 2, error bars show the range. (E) Residual versus simulation results and (F) versus time show predictable behavior in the later points. (Color version of figure is available online.)

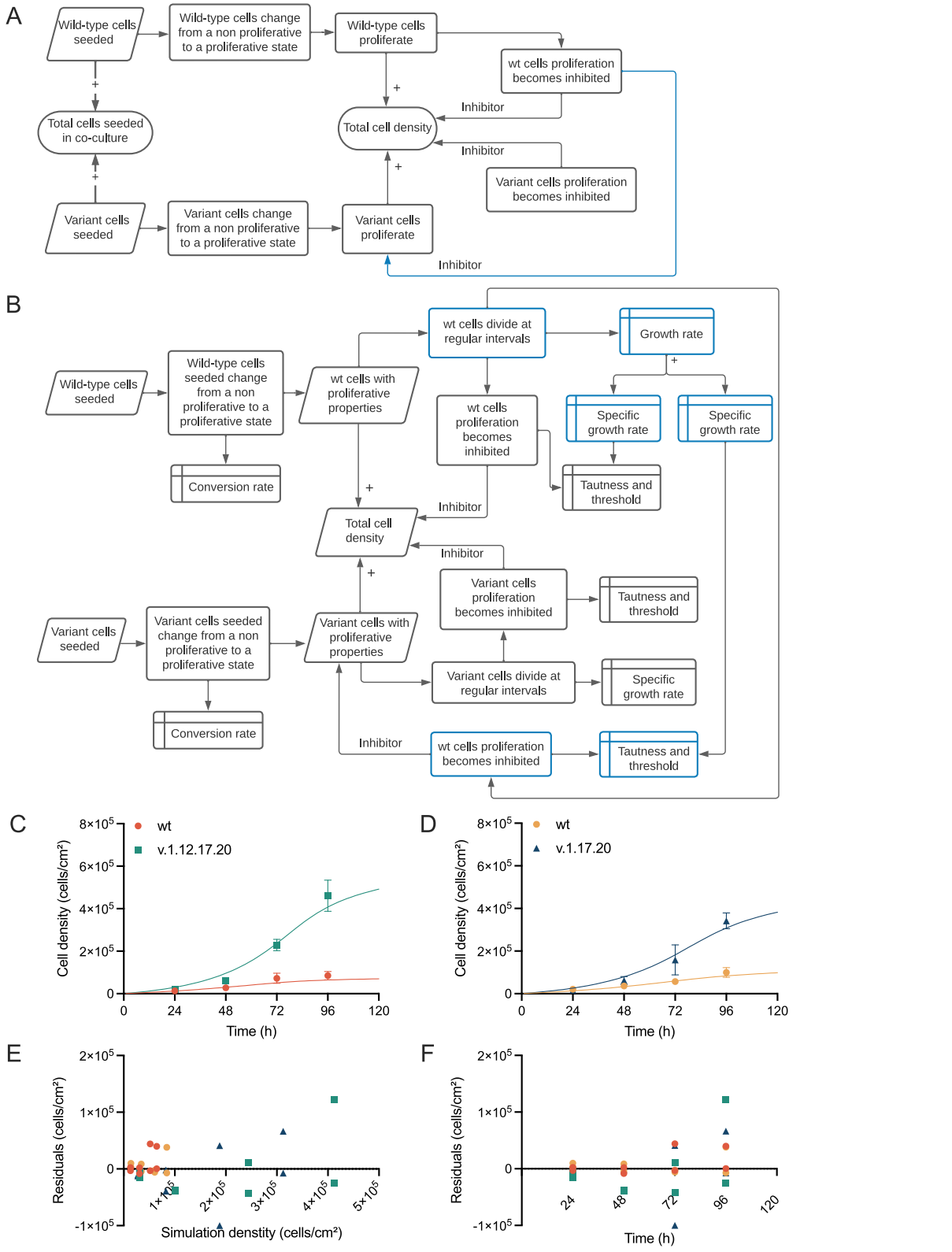

Figure 3. (A) Co-culture representation, incorporating the variant's growth inhibitor effect over the wild-type, and (B) the software building blocks to represent the behavior. Simulation results (line) and experimental counts (markers) across time for the restructured model representing the co-culture of the (C) wild-type and v.1.12.17.20 and (D) wild-type-RFP and v.1.17.20 populations. N = 2, error bars show the range. (E) Residual versus simulation results and (F) versus time do not display predictability. (Color version of figure is available online.)

Table 3
Fitted parameters that characterized the conditions in the restructured model.

Condition		1		2	
Parameter	Variable	wild-type	v.1.12.17.20	wild-type	v.1.17.20
Conversion of cell state rate, h^{-1}	Eqs. 8 and 9, r_r	*2*	*2*	*2*	*2*
Cell density inhibits wild-type and variant populations					
Specific growth rate, h^{-1}	Eqs. 10 and 11, r_g	**0.018**	*0.035*	**0.02**	*0.032*
Inhibition sensitivity, $\times 10^{-5}$ cm^2 /cells	Eqs. 10 and 11, g_s	*1.0*	*1.5*	*1.0*	*1.5*
Inhibition threshold, $\times 10^5$ cells/cm^2	Eqs. 10 and 11, g_c	*3.9*	*4.7*	*3.9*	*4.1*
The presence of variants inhibits the wild-type population					
Specific growth rate, h^{-1}	Eq. 10, r_h	**0.003**	–	**0.002**	–
Inhibition sensitivity, $\times 10^{-5}$ cm^2 /cells	Eq. 10, g_y	**1.5**	–	**6**	–
Inhibition threshold, $\times 10^3$ cells/cm^2	Eq. 10, g_x	**7**	–	**4.5**	–

The optimized parameter values are displayed in bold, and the manually assigned (obtained from the monoculture model) are shown in italics.

manufacturing control, we simulated the effect of variant hPSCs across a range of culture parameters (Table 1). We calculated the overall culture density and proportion of variants at various passages, as well as the variant overgrowth rate ($\triangle\mu$) over each passage interval (according to Equation 13). In line with previous findings, a culture system with the presence of variants is subject to a variant overgrowth. The effect of this variant overgrowth rate increases both as the overall density and the proportion of variants increases. Underpinning the overgrowth is the variant cells higher growth rate in comparison with wild-type hPSCs and the earlier density mediated inhibition of the wild-type population than that of the variant. However, we noted as the culture becomes more confluent the variant also becomes inhibited, and thus its overgrowth rate starts to decrease (Figure 5). Overall, our model demonstrates that the rate at which variant cells overtake a wild-type population can be predicted at given process parameters when the growth behavior of both wild-type and variant hPSC populations is known.

Discussion

Manufacturing of hPSC-based cell therapy requires an understanding of the culture parameters that control the expansion of genetically variant cells, as they have the potential to compromise operational processes [4,5]. Here, we report that the independent growth behavior as well as the selective growth and competitive advantage of genetically variant hPSCs can be mathematically represented using an ODE framework.

Our model showed how the system parameters controlling independent growth behavior of wild-type and genetic variant populations are altered when both populations exist within a co-culture environment. Furthermore, our model revealed that under the presence of variants, cell behavior changes with the state of the culture. The data generated showed that wild-type cells experience a variant overgrowth rate, and this overgrowth increases as the culture system becomes more confluent. Moreover, the low degree of representation obtained of wild-type cells at low densities in the co-culture model, mainly under-predicting the behavior, suggests that cells are less susceptible to experiencing an inhibition driven by variants at low densities.

Alternative models cited in the literature (in particular the generalized logistic model, or the competitive generalized logistic model) would likely have produced a similar outcome based on similar mechanistic routes [19]. We have favored the ODE approach described due to the clear attribution of each parameter to a biological behavior. This facilitates mechanistic analysis of cause-and-effect as well as future development of the model to cover wider scenarios (such as a cell death phase). We have previously described this building block approach to modeling biomanufacture systems and the advantages we believe it holds in communication in multidisciplinary environments.

Of particular value, these observations lead to an operational scenario whereby controlling the state of the culture could determine the outcomes of the process. Use of operational protocols that operate in the low-density region would permit scenarios in which wild-type cells experience less variant-mediated inhibition. Thus, the culture system would consequently have a lower variant overgrowth rate effect, thereby reducing the rate at which variant hPSCs can overtake wild-type cells.

The ability of our computational model to quantify cell behavior opens the opportunity to define future operational scenarios. Although only two genetically variant sublines were employed in this study, as our knowledge of other undesirable variants becomes clearer, manufacturers will need to know how quickly arising variants reach the threshold for detection and the value of this point in their manufacturing trains. In this scenario, protocols could be designed to operate at high densities, enabling the system to experience a higher overgrowth rate that would permit faster detection of genetic mosaicism [3].

In manufacture of a hPSC-based cell therapy, a timely detection of variants is important for product release and de-risking the therapies. The modeling system developed in this study could be applied in two complementary different ways to facilitate the timely detection of variants arising in hPSC cultures. First, tracking the growth patterns of expanding cultures would enable the detection of variant hPSCs by identifying a deviation of growth characteristics outside the biological variability of the culture system predicted by the model. Additionally, a useful manner for using this resource would be to deliberately subject a duplicate culture to conditions predicted by the model to facilitate overtake of variant cells. If present in culture, variants should reach the threshold required for detection by genetic or modeling methods (e.g., growth rates as explained previously) more quickly, thus allowing more timely detection of their potential presence in hPSC populations destined for clinical use.

We note that in the final version of our model there is the indication that further model parameters are required to more precisely represent wild-type and variant cell behavior at lower density values. Designing these experiments is particularly important for defining the rate of emergence of a new variant that will initially be a single cell. Although not evaluated in this study, the set-up of these experiments could be easily designed and enriched by computational models, requiring only changes to the input variables to establish the experimental conditions that could provide a better understanding of the system (e.g., seeding densities, passage number). At the same time, the knowledge gained from these experiments could facilitate building the computational model further, leading to an iterative experimental and simulation research cycle.

In conclusion, our work has shown how computational models can help unlock complex biological systems by generating new insights about the mechanisms driving these behaviors and testing

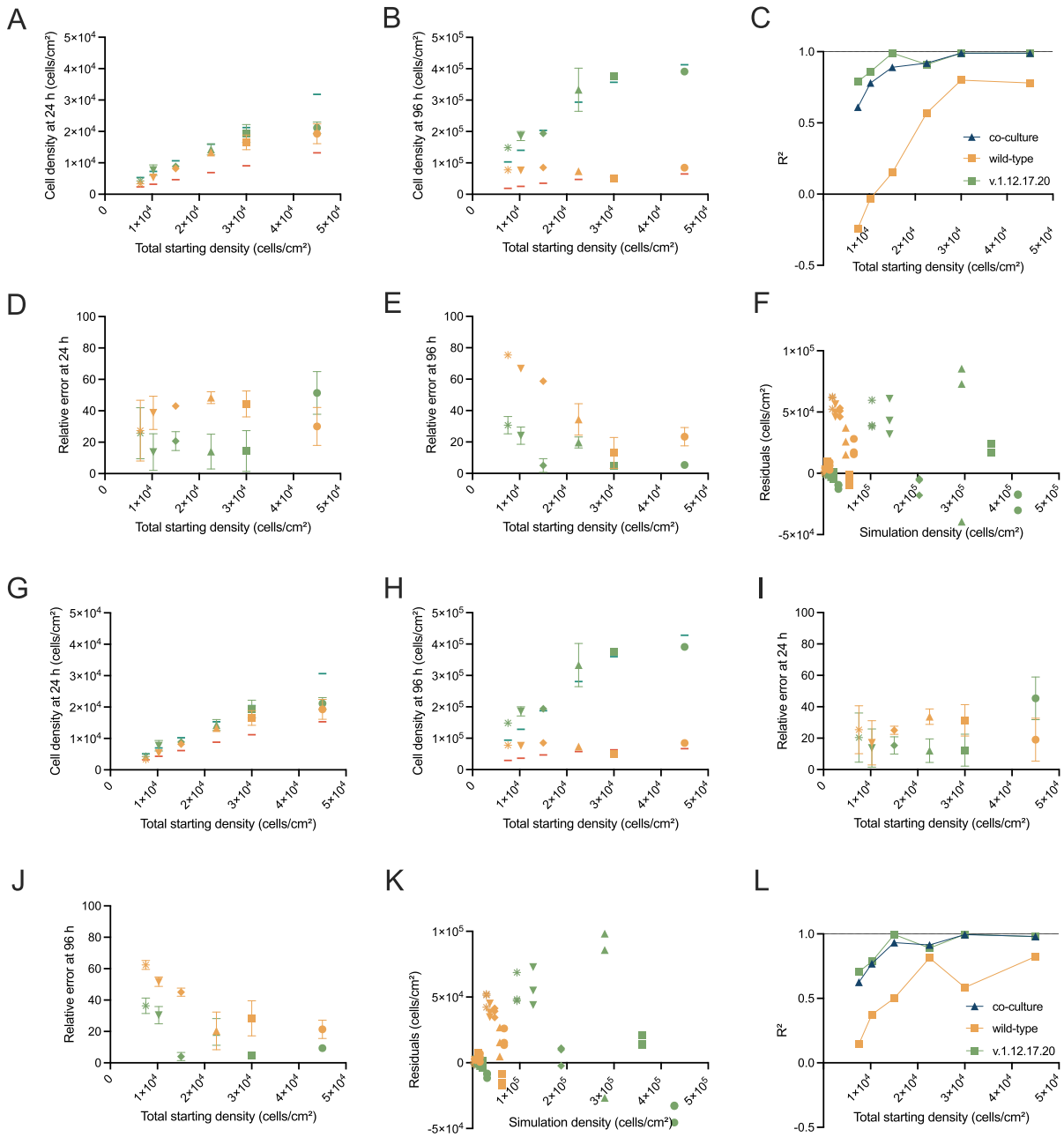

Cell line	wild-type	variant	wild-type	variant	wild-type	variant	wild-type	variant	wild-type	variant	wild-type	variant
Condition	●	●	■	■	▲	▲	◆	◆	▼	▼	✳	✳
Density (x10⁴)	4.5		3.0		2.25		1.5		1.025		0.75	

Figure 4. Simulation results (line) and experimental counts (markers) across starting densities representing a new data set at (A) 24 and (B) 96 h of culture. N = 3, error bars show SD. (C) Residual versus simulation results. Relative error between the simulation and experimental results at (D) 24 and (E) 96 h of culture. (F) R^2 across starting densities for the co-culture representation and the representation of each population in co-culture. Simulation results (line) and experimental counts (markers) across starting densities represented with the fitted parameters at (G) 24 and (H) 96 h of culture, and their relative error (I) and (J). N =3, error bars show SD. (K) Residuals versus simulation results. (L) R^2 across starting densities for the co-culture representation. SD, standard deviation. (Color version of figure is available online.)

Table 4
Fitted parameter values that characterize both populations seeded at different proportions.

Parameter	Variable	Wild-type	v.1.12.17.20
Conversion of cell state rate, h^{-1}	Eqs. 8 and 9, r_r	*2*	*2*
Cell density inhibits wild-type and variant populations			
Specific growth rate, h^{-1}	Eqs. 10 and 11, r_g	**0.018**	**0.034**
Inhibition sensitivity, $\times 10^{-5}$ cm^2/cells	Eqs. 10 and 11, g_s	**1.0**	**2.5**
Inhibition threshold, $\times 10^5$ cells/cm^2	Eqs. 10 and 11, g_c	**3.6**	**5.0**
The presence of variants inhibits the wild-type population			
Specific growth rate, h^{-1}	Eq. 10, r_h	**0.013**	–
Inhibition sensitivity, $\times 10^{-5}$ cm^2/cells	Eq. 10, g_y	**2.5**	–
Inhibition threshold, $\times 10^3$ cells/cm^2	Eq. 10, g_x	**13**	–

The optimized parameter values are displayed in bold, and the manually assigned (obtained from the monoculture model) are shown in italics.

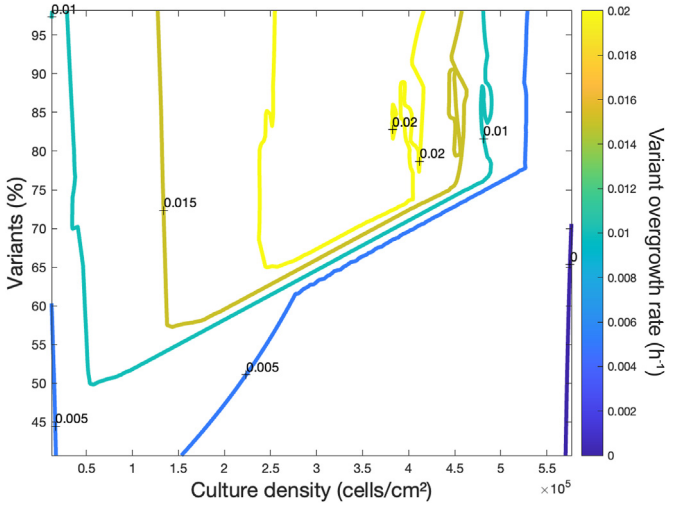

Figure 5. Relationship between culture density, percentage of variants and variant overgrowth rate shows that variants intrinsically experience an overgrowth in co-culture. The variant overgrowth rate is represented in the color-scale bar. (Color version of figure is available online.)

hypotheses. Moreover, it has demonstrated that the ODE modeling framework can represent the complexity of cell dynamics to an acceptable degree for manufacturing applications. Undertaking future studies to assess the degree of representation under a wider range of conditions generating more diverse growth rates across wild-type and variant cells will provide further insight into mechanisms driving variant's competitive growth advantage.

Declaration of Competing Interest

The authors have no commercial, proprietary or financial interest in the products or companies described in this article.

Funding

This work was supported by the Medical Research Council MR/N009371/1, MR/X000028/1 and the UK Regenerative Medicine Platform, MRC reference MR/R015724/1.

Author Contributions

Conception and design of the study: CBR, CJP, IB and RJT. Acquisition of data: CBR and CJP. Analysis and interpretation of data: CBR, CJP, KG, IB and RJT. Drafting or revising the manuscript: CBR, CJP, AS, IB, KG and RJT. All authors have approved the final article.

Acknowledgments

The authors thank Sheffield Genetics Diagnostic Service for cytogenetic analyses.

References

[1] Kim JY, Nam Y, Rim YA, Ju JH. Review of the current trends in clinical trials involving induced pluripotent stem cells. Stem Cell Reviews and Reports 2022;18:142–54.
[2] Bashor CJ, Hilton IB, Bandukwala H, Smith DM, Veiseh O. Engineering the next generation of cell-based therapeutics. Nature Reviews. Drug Discovery 2022;21:655–75.
[3] Wiegand C, Banerjee I. Recent advances in the applications of iPSC technology. Current Opinion in Biotechnology 2019;60:250–8.
[4] Baker DE, et al. Adaptation to culture of human embryonic stem cells and oncogenesis in vivo. Nature Biotechnology 2007;25:207–15.
[5] Halliwell J, Barbaric I, Andrews PW. Acquired genetic changes in human pluripotent stem cells: origins and consequences. Nature Reviews. Molecular Cell Biology 2020;21:715–28.
[6] Draper JS, et al. Recurrent gain of chromosomes 17q and 12 in cultured human embryonic stem cells. Nature Biotechnology 2004;22:53–4.
[7] Baker D, et al. Detecting genetic mosaicism in cultures of human pluripotent stem cells. Stem Cell Reports 2016;7:998–1012.
[8] International Stem Cell Initiative. Screening ethnically diverse human embryonic stem cells identifies a chromosome 20 minimal amplicon conferring growth advantage. Nature Biotechnology 2011;29:1132–44.
[9] Liang G, Zhang Y. Genetic and epigenetic variations in iPSCs: potential causes and implications for application. Cell Stem Cell 2013;13:149–59.
[10] Price CJ, et al. Genetically variant human pluripotent stem cells selectively eliminate wild-type counterparts through yap-mediated cell competition. Developmental Cell 2021;56:2455–70.
[11] Turinetto V, Orlando L, Giachino C. Induced pluripotent stem cells: advances in the quest for genetic stability during reprogramming process. International Journal of Molecular Sciences 2017;18:1952–19780.
[12] Price CJ, Barbaric I. Assessing cell competition in human pluripotent stem cell (HPSC) cultures. Current Protocols 2022;2:e435.
[13] Stacey AJ, Cheeseman EA, Glen KE, Moore RL, Thomas RJ. Experimentally integrated dynamic modelling for intuitive optimisation of cell based processes and manufacture. Biochemical Engineering Journal 2018;132:130–8.
[14] Glen KE, Cheeseman EA, Stacey AJ, Thomas RJ. A mechanistic model of erythroblast growth inhibition providing a framework for optimisation of cell therapy manufacturing. Biochemical Engineering Journal 2018;133:28–38.
[15] Shariatzadeh M, Lopes AG, Glen KE, Sinclair A, Thomas RJ. Application of a simple unstructured kinetic and cost of goods models to support T-cell therapy manufacture. Biotechnology Progress 2021;37:e3205–20.
[16] Thomson JA, et al. Embryonic stem cell lines derived from human blastocysts. Science (New York, N.Y.) 1998;282:1145–7.
[17] Laing O, Halliwell J, Barbaric I. Rapid PCR assay for detecting common genetic variants arising in human pluripotent stem cell cultures. Protoc Stem Cell Biol 2019;49:e83.
[18] Chen G, et al. Chemically defined conditions for human iPS cell derivation and culture. Nature methods 2011;8:424–9.
[19] Wachenheim DE, Patterson JA, Ladisch MR. Analysis of the logistic function model: derivation and applications specific to batch cultured microorganisms. Bioresource Technology 2003;86:157–64.